ACS APPLIED MATERIALS & INTERFACES

Research Article

www.acsami.org

Temperature Dependent Phonon Shifts in Single-Layer WS_2

Thripuranthaka M. and Dattatray J. Late*

Physical & Materials Chemistry Division, CSIR-National Chemical Laboratory, Dr. Homi Babha Road, Pashan, Pune 411008, India

Supporting Information

ABSTRACT: Atomically thin two-dimensional tungsten disulfide (WS_2) sheets have attracted much attention due to their potential for future nanoelectronic device applications. We report first experimental investigation on temperature dependent Raman spectra of single-layer WS_2 prepared using micromechanical exfoliation. Our temperature dependent Raman spectroscopy results shows that the E^1_{2g} and A_{1g} modes of single-layer WS_2 soften as temperature increases from 77 to 623 K. The calculated temperature coefficients of the frequencies of 2LA(M), E^1_{2g}, A_{1g}, and A_{1g}(M) + LA(M) modes of single-layer WS_2 were observed to be −0.008, −0.006, −0.006, and −0.01 cm^{-1} K^{-1}, respectively. The results were explained in terms of a double resonance process which is active in atomically thin nanosheet. This process can also be largely applicable in other emerging single-layer materials.

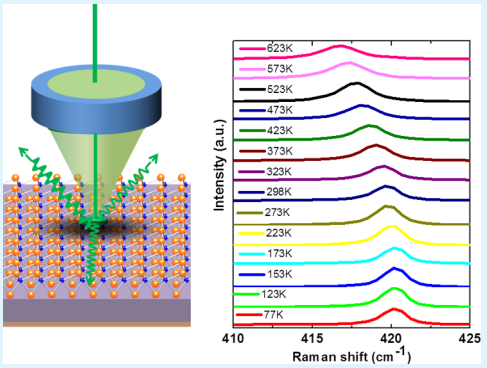

KEYWORDS: *WS_2, layered materials, Raman spectroscopy, phonon vibrations, thermal effect*

INTRODUCTION

Two-dimensional (2D) atomically thin layered materials such as graphene[1−6] and monolayer transition metal dichalcogenides (TMDCs) such as MX_2 (M = Mo, W and X = Se, S) are currently an intriguing great interest as 2D semiconductors with rich physical and chemical properties as native direct energy gap in visible frequency range and has potential to be used in future nanoelectronic device applications. Graphene-based transistors have been extensively explored for their potential use in various nanoelectronic applications such as logic and radio frequency devices.[5,6] The main advantage of single-layer graphene (SLG) based field-effect transistors (FET) is high carrier mobility.[5,6] However, due to absence of a bandgap, several problems still remain with SLG, which is essential to make transistor device on and off. Therefore, single layers of other TMDCs semiconductor layered materials such as MoS_2,[7−16] WS_2,[17−21] WSe_2,[21−23] $MoSe_2$,[24−27] GaS,[11,28] and GaSe[11,28] are gaining increasing attention from scientific community in worldwide as promising new materials for FET, integrated optoelectronic circuits, photo detectors, sensors, etc. Another advantage of single-layer TMDCs semiconductor materials is direct and wide bandgap versus narrow and indirect bandgap in bulk form. There are complete and exhaustive investigations on single-layer MoS_2 including various properties such as optical and electronic properties, strain effects, thermal effects, and so on. However, investigation on WS_2 has just begun, similar layered materials as of 2H-MoS_2, single-layer 2H-WS_2 were made up of sandwiching two sulfur atoms and one W atom through covalent bonds of W−S, forming S−W−S structure. Bulk WS_2 is an indirect semiconductor material when it is thin to a monolayer sheet, the bandgap becomes wider and direct ∼2 eV at the corners (K and K′ points) of the Brillion Zone as predicted by both theoretical calculations and experimental investigations.[21−23] All these interesting properties revealed that WS_2 is a potential candidate for next generation nanoelectronic device applications.

The atomically thin WS_2 nanosheet is a promising candidate material from a technology point of view as it has been recently reported as vertical FETs incorporating graphene−WS_2 which offer the possibility of flexible and transparent electronic devices[18] and photosensor devices.[20] In view of gaining attention of single-layer WS_2 for possible application in various nanoelectronic devices, it is important to investigate the electron−phonon (e−p) interaction and vibrational properties of single-layer WS_2 based various nanoelectronic devices. It is considered that applying the bias and the back gate voltage results in self-heating of the device which can affect performance of atomically thin layered WS_2 based nanoelectronic devices. The self-heating may result in a change of the e−p interaction and vibrational properties. It is important to know the changes in Raman spectra peak positions and shape of the peak with temperature in order to distinguish them from the changes due to the other factors such as number of atomic layers, etc. However, temperature-dependent Raman spectroscopy of single-layer WS_2 has not been reported until now in the literature. It is important to understand the physical, mechanical, and chemical properties of a single-layer WS_2 nanosheet. Raman spectroscopy is widely and nondestructively used to measure the number of atomic layers and mechanical and thermal properties of graphene and various inorganic layered materials.[1−28]

The temperature coefficients of the Raman-active peaks in single-layered WS_2 were different from those of the multilayer sample. It can be used to differentiate single-layer WS_2 samples among multilayer sample in the device application point of view.

Received: October 31, 2013
Accepted: December 23, 2013
Published: December 23, 2013

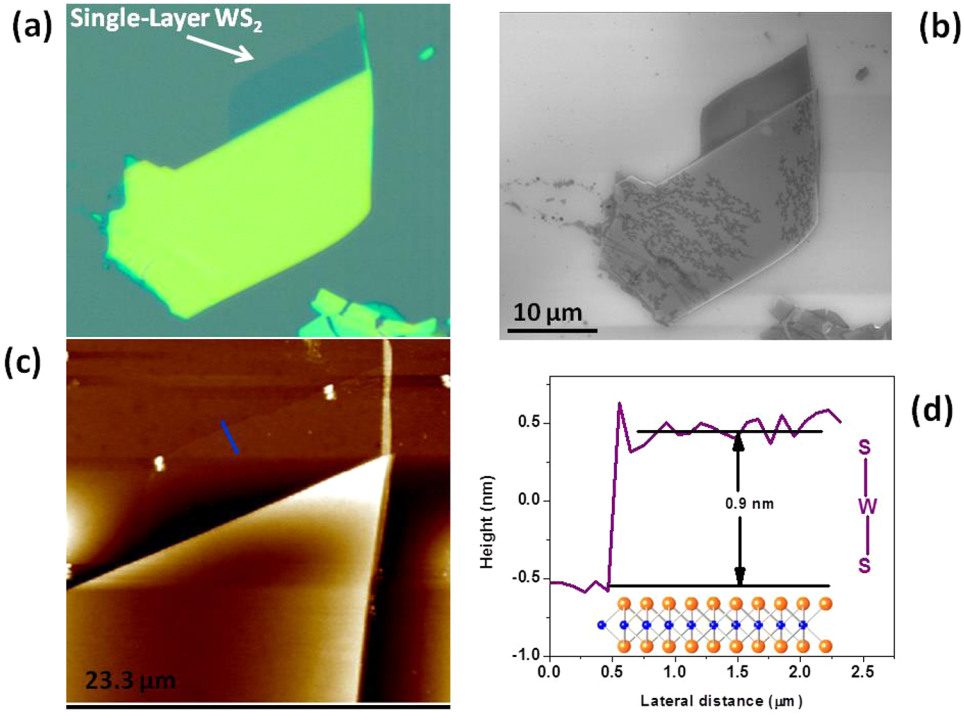

Figure 1. Single-layer WS_2 (a) optical image, (b) SEM image, (c) AFM image, and (d) corresponding AFM height profile.

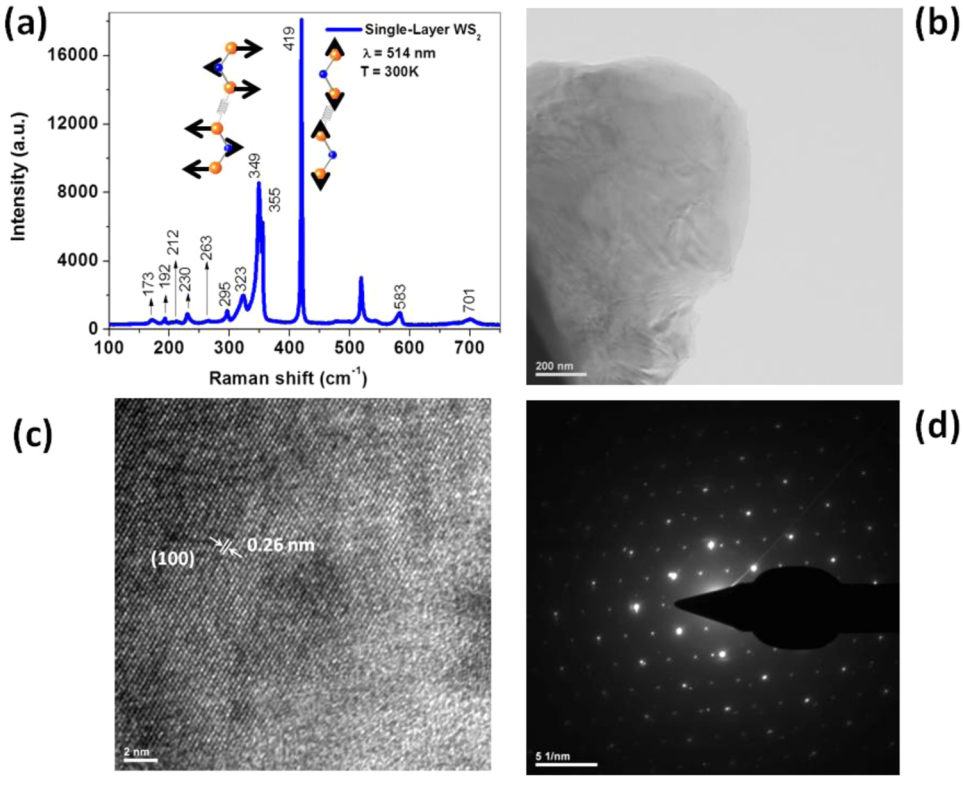

Figure 2. (a) Room temperature Raman spectra of single-layer WS_2. (b) High resolution TEM image of few layers WS_2. (c) HRTEM image of few layers WS_2 and (d) corresponding SAED pattern of WS_2.

Due to variation in temperature, the Raman-active peaks also get affected with electron-phonon coupling. This can also lead to affect the field effect mobility of the WS_2 transistor based devices. Here, we demonstrate for the first time temperature dependent Raman spectroscopy of single-layer WS_2 with temperature ranging from 77 to 623 K.

RESULTS AND DISCUSSION

Figure 1a shows the optical image of the single-layer and multilayer sheet of WS_2 prepared using micromechanical scotch tape technique onto 300 nm SiO_2/Si substrate. Figure 1b shows the scanning electron microscope (SEM) image of the single-layer

dx.doi.org/10.1021/am404847d | ACS Appl. Mater. Interfaces 2014, 6, 1158−1163

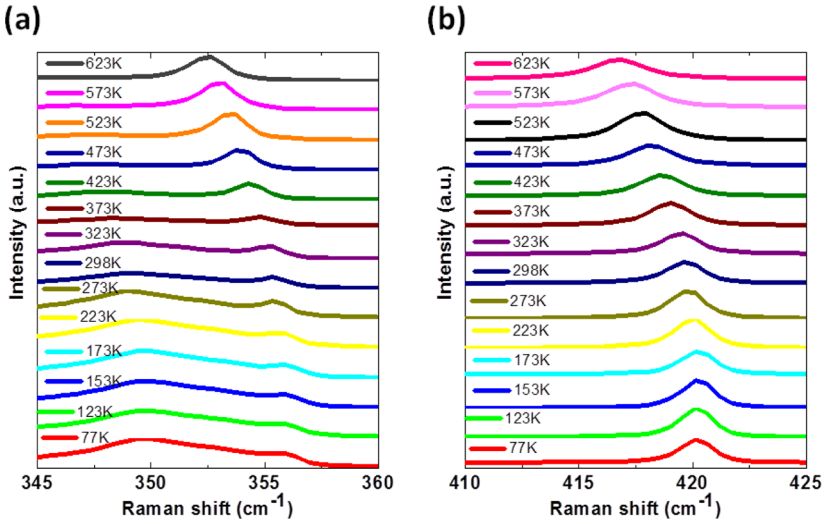

Figure 3. Raman spectra of single-layer WS_2 with (a) E^1_{2g} and (b) A_{1g} mode measured in a temperature range from 77 to 623 K.

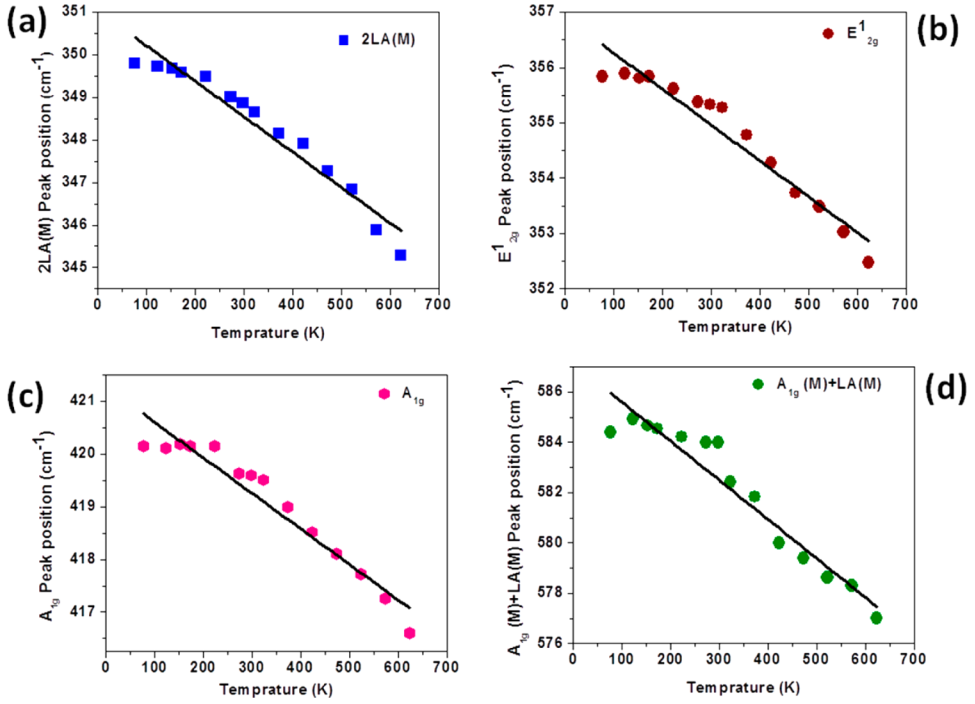

Figure 4. Effect of temperature variation on the Raman frequencies of single-layer WS_2 for (a) 2LA(M), (b) E^1_{2g}, (c) A_{1g} mode, and (d) A_{1g} (M) + LA(M).

and multilayer WS_2 sheet corresponds to optical image shown in a. Figure 1c shows the atomic force microscopy (AFM) image of single-layer WS_2, and Figure 1d shows the corresponding AFM height profile. The measured thickness of the sheet was observed to be ~0.9 nm which indicates the single-layer nature of WS_2. Raman spectrum of single-layer and multilayer WS_2 show the thickness dependence of in-plane (E^1_{2g}) and out-of-plane (A_{1g}) Raman modes along with both modes shifting away from each other in frequency with increasing thickness as due to the double resonance scattering which can be the spectral finger print of single-layer WS_2.[29] Figure 2a shows the typical Raman spectrum of single-layer WS_2 over a frequency range of 100−750 cm^{-1} recorded at room temperature using 514.5 nm laser. Raman spectra of single-layer WS_2 excited using 514.5 nm were consist

Table 1. Extracted Temperature Coefficient and Frequency Difference for Single-Layer WS_2 Nanosheet

single-layer WS_2	χ (cm^{-1} K^{-1})	$\Delta\omega$
2LA(M)	−0.008 ± 0.0009	4.5 ± 0.50
E^1_{2g}	−0.006 ± 0.0005	3.3 ± 0.40
A_{1g}	−0.006 ± 0.0009	3.5 ± 0.45
A_{1g}(M) + LA(M)	−0.01 ± 0.006	7.4 ± 0.80

of many first-order and second-order peaks namely LA(M) which appears at 173 cm^{-1}, A_{1g}(M)−LA(M) which appears at 230 cm^{-1}, 2LA(M)−$3E^2_{2g}$ (M) which appears at 263 cm^{-1}, 2LA(M)−$2E^2$−$2E^2_{2g}$ (M) which appears at 295 cm^{-1}, 2LA(M) which appears at 349 cm^{-1}, E^1_{2g} appears at 355 cm^{-1}, A_{1g} appears at 419 cm^{-1}, A_{1g} (M) + LA(M) which appears at 583 cm^{-1}, and

dx.doi.org/10.1021/am404847d | ACS Appl. Mater. Interfaces 2014, 6, 1158−1163

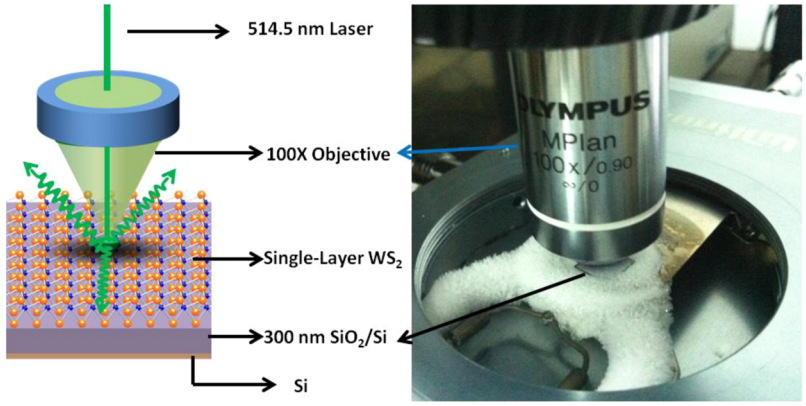

Figure 5. Experimental setup of temperature dependent Raman spectroscopy of single-layer WS_2 (a) schematic diagram and (b) optical photograph.

4LA(M) which appears at 701 cm^{-1}. The 2LA (M) mode and E^1_{2g} mode overlap with each other. Our Raman spectra of single-layer WS_2 are in good agreement with that reported earlier by Berkdemir et al.[19] Figure 2b and c show the low and high resolution TEM images of few layer WS_2 nanosheets prepared using micromechanical exfoliation from bulk WS_2 crystal transferred directly onto Quanta foil TEM grid. TEM shows high crystalline quality and the sheet like morphology with some wrinkles on WS_2 sheet surface. Figure 2d shows the corresponding selected area electron diffraction pattern of few layer thick WS_2 sheet.

Figure 3a shows the Raman spectra of single-layer WS_2 with 2LA(M) and E^1_{2g} modes as a function of temperature from 77 to 623 K. Figure 3b shows the Raman spectra of single-layer WS_2 for A_{1g} mode as a function of change in temperature. Raman spectra of single-layer WS_2 for A_{1g}(M) + LA(M) are shown in the Supporting Information Figure S1b. Further, it has been observed that all Raman modes of single-layer WS_2 2LA(M), E^1_{2g}, A_{1g}, and A_{1g}(M) + LA(M) change linearly as a function of temperature variation as shown in Figure 4a−d. It is known that the Raman spectroscopy is a four-phonon process which is dominant over thermal expansion as well as the three phonon process on E^1_{2g} and A_{1g} mode line shift with change in temperature (Table 1). The changes in Raman mode frequencies $\Delta\omega$, with temperature variation from 77 to 623 K were observed to be 4.5 cm^{-1} for 2LA(M), 3.3 cm^{-1} for E^1_{2g}, 3.5 cm^{-1} for A_{1g}, and 7.4 cm^{-1} for A_{1g}(M) + LA(M) mode, respectively. Some data points spreading for the Raman peak positions were noticed which may be due to change of laser spot on single-layer WS_2 sheet, or local Raman stage vibration and low excitation power on the single-layer WS_2 sheet surface followed by extra attenuation from cold-hot cell window. The temperature dependence Raman spectra were yet carried out on several other single-layered WS_2 sample, and all results were found to be similar in nature. The observed data of the peak positions obtained from Lorentzian fittings for 2LA(M), E^1_{2g}, A_{1g}, and A_{1g}(M) + LA(M) mode versus temperature were fitted using Grüneisen model[30]

$$\omega(T) = \omega o + \chi T \quad (1)$$

where ωo is the peak position of vibration 2LA(M), E^1_{2g}, A_{1g}, or A_{1g}(M) + LA(M) modes at 0 K temperature and χ is the first-order temperature coefficient of the 2LA(M), E^1_{2g}, A_{1g}, or A_{1g}(M) + LA(M) modes. The plot of 2LA(M), E^1_{2g}, A_{1g}, or A_{1g}(M) + LA(M) versus temperature gives slope of the fitted straight line which depicts the temperature coefficient χ. The temperature coefficients of the frequencies of the 2LA(M), E^1_{2g}, A_{1g}, and A_{1g}(M) + LA(M) bands of single- layer WS_2 are observed to be −0.008, −0.006, −0.006, −0.01 cm^{-1} K^{-1}, respectively. Table 1 depicts the summary of extracted temperature coefficient and frequency difference for single-layer WS_2 nanosheet. It is important and surprising to note herewith that the temperature coefficient of single-layer WS_2 for both E^1_{2g} and A_{1g} mode were observed to be identical. In other hand temperature coefficient for A_{1g}(M) + LA(M) mode were observed to be high. Our temperature coefficient values of E^1_{2g} and A_{1g} modes were observed to be one order smaller than those reported for single-layer and few-layer MoS_2 by Lanzillo et al.,[31] Sahoo et al.,[32] and Najmaei et al.[33] The presence of substrate 300 nm SiO_2/Si which we have used in present investigation to support single-layer WS_2 may not contribute in final results of temperature coefficients. We believe that E^1_{2g} mode in single-layer WS_2 represents in-plane vibration mode which will restrict motion of W and S atoms in plane of sheet. Also it is important to note that the full width at half maxima (FWHM) of all modes 2LA(M), E^1_{2g}, A_{1g}, and A_{1g}(M) + LA(M) increases with increasing temperature for single-layer WS_2. The observed behavior may be due to result of phonon−phonon interaction which involves a phonon decaying into lower-energy phonons and electron−phonon interaction which results from a phonon generating an electron−hole (e−p) pair. Further, the variation in the Raman spectra peak position as a function of temperature in single-layer WS_2 sheet is due to the temperature contribution that consequences from anharmonicity and contribution from the thermal expansion or volume contribution. This is also due to the contributation from a double resonance phenomenon which is active only in atomically thin sheet.

CONCLUSIONS

In conclusion, we have systematically investigated the temperature-dependent Raman spectroscopy for single-layer WS_2 with wide temperature range from 77 to 623 K. All first- and second-order modes of single-layer WS_2 soften as a function of increasing temperature. The calculated temperature coefficients of the frequencies of the 2LA(M), E^1_{2g}, A_{1g}, and A_{1g}(M) + LA(M) bands of single-layer WS_2 are observed to be −0.008, −0.006, −0.006, −0.01 cm^{-1} K^{-1}, respectively. The results were explained in terms of a double resonance process which is active in single-layer sheet. We believe that the work reported in this paper could be extended to other two-dimensional single-layer materials and enrich the knowledge of these promising materials for specific application.

dx.doi.org/10.1021/am404847d | ACS Appl. Mater. Interfaces 2014, 6, 1158−1163

EXPERIMENTAL METHODS

Preparation of Single-Layer WS_2. Bulk WS_2 crystal were Purchased from MoS_2 crystal Supplies Inc., UK, (Crystal size small). Single-layer and few layers of WS_2 sheets were deposited at room temperature in ambient conditions by mechanically exfoliating bulk WS_2 crystal onto pre-cleaned 300 nm SiO_2/Si as described earlier for single-layer MoS_2.[15] The only difference observed here was light brown color of WS_2 flakes on scotch tape. Finally, the scotch-tape which was transferred during exfoliation on substrates was removed by dipping the substrates in acetone for 5 min.

Optical Microscope. Nikon LV150NL Trinocular upright optical microscope with an imager M1m was used to locate the single-layer of WS_2 sheets deposited on 300 nm SiO_2/Si substrates using specific color contrast. The color images were acquired with LED illumination and using bright field imaging modes with MTI plan EPI 100× objectives and 10× eyepiece. The exposure times were varied in the range 10−500 ms depending upon the filter used.

Atomic Force Microscope (AFM). AFM tapping mode images were recorded using an ICON system (Bruker, Santa Barbara Ca.).

Raman Spectsocopy. The Raman spectra of single-layer WS_2 prepared using micromechanical exfoliation of bulk WS_2 crystal were used to investigate temperature dependent Raman with a (LabRAM HR) using Ar laser (514.5 nm) in the back scattering geometry. The detector was a Synapse CCD detector with thermoelectric cooling to −70 °C. A 50× objective were used to focus the laser beam and to collect the Raman signal. The laser power on the sample was ∼500 μW for 514.5 nm, to avoid possible heating effect by the laser on sheet surface. The size of the laser spot was ∼1 μm. Figure 5 shows the experimental set-up of temperature dependent Raman spectroscopy of single-layer WS_2. All the Raman spectra were obtained under the same experimental conditions, and the band positions and widths were obtained by fitting them with a Lorentzian function.

FESEM. Field emission (FE) SEM images were collected using FEI ESEM QUANTA Instruments.

HR-TEM. HR-TEM images were acquired using FEI TECNAI TF-30 (FEG) instrument.

ASSOCIATED CONTENT

Supporting Information

Temperature-dependent Raman spectra for single-layer WS_2 with A1g (M) + LA (M) mode (Figure S1), comparative Raman spectra of bulk and single-layer WS_2 (Figure S2), and AFM image of single-layer WS_2 (Figure S3). This material is available free of charge via the Internet at http://pubs.acs.org.

AUTHOR INFORMATION

Corresponding Author

*E-mail: dj.late@ncl.res.in and datta099@gmail.com.

Author Contributions

D.J.L. designed the experiment, supervised the overall investigations, carried out the experimental work, data analysis, and wrote the manuscript. T.M. carried out the experimental work. All authors have given approval to the final version of the manuscript.

Notes

The authors declare no competing financial interest.

ACKNOWLEDGMENTS

One of the authors, D.J.L., would like to thank DST (Government of India) for the Ramanujan fellowship. The research was primarily supported by NCL-MRP project grant MLP 028626. Partial support by DST Fast Track scheme for Young scientist project is gratefully acknowledged. The authors would like to thank Prof. C. N. R. Rao, FRS (Director, ICMS & Founder President JNCASR Bangalore), Prof. Vinayak P. Dravid (Northwestern University, USA), and Director CSIR-NCL for constant support and encouragement.

REFERENCES

(1) Novoselov, K. S.; Geim, A. K.; Morozov, S. V.; Jiang, D.; Zhang, Y.; Dubonos, S. V.; Grigorieva, I. V.; Firsov, A. A. *Science* **2004**, *306*, 666−669.
(2) Novoselov, K. S.; Jiang, D.; Schedin, F.; Booth, T. J.; Khotkevich, V. V.; Morozov, S.V.; Geim, A. K. *Proc. Nat. Acad. Sci.* **2005**, *102*, 10451−10453.
(3) Ghosh, A.; Late, D. J.; Panchakarla, L.S.; Govindaraj, A.; Rao, C. N. R. *J. Exp. Nanosci.* **2009**, *4*, 313−322.
(4) Late, D. J.; Maitra, U.; Panchakarla, L. S.; Waghmare, U. V.; Rao, C. N. R. *J. Phys.: Condens. Matter* **2011**, *23*, 055303.
(5) Schwierz, F. *Nat. Nanotech.* **2010**, *5*, 487−496.
(6) Avouris, P.; Chen, Z.; Perebeinos, V. *Nat. Nanotechnol.* **2007**, *2*, 605.
(7) Radisavljevic, B.; Radenovic, A.; Brivio1, J.; Giacometti, V.; Kis, A. *Nature Nanotechnol.* **2011**, *6*, 147−150.
(8) Wang, H.; Yu, L.; Lee, Y.; Shi, Y.; Hsu, A.; Chin, M. L.; Li, L.; Dubey, M.; Kong, J.; Palacios, T. *Nano Lett.* **2012**, *12*, 4674−4680.
(9) Jariwala, D.; Sangwan, V. K.; Late, D. J; Johns, J. E.; Dravid, V. P.; Marks, T. J.; Lauhon, L. J.; Hersam, M. C. *Appl. Phys. Lett.* **2013**, *102*, 173107.
(10) Matte, H. S. S. R.; Gomathi, A.; Manna, A. K.; Late, D. J.; Datta, R.; Pati, S. K.; Rao, C. N. R. *Angew. Chem. Int. Ed.* **2010**, *49*, 4059−4062.
(11) Late, D. J.; Liu, B.; Matte, H. S. S. R.; Rao, C. N. R.; Dravid, V. P. *Adv. Fun. Mater.* **2012**, *22*, 1894−1906.
(12) Yin, Z.; Li, H.; Li, H.; Jiang, L.; Shi, Y.; Sun, Y.; Lu, G.; Zhang, Q.; Chen, X.; Zhang, H. *ACS Nano* **2012**, *6*, 74−80.
(13) Ghatak, S.; Pal, A. N.; Ghosh, A. *ACS Nano* **2011**, *5*, 7707−7712.
(14) Late, D. J.; Liu, B.; Matte, H. S. S. R.; Dravid, V. P.; Rao, C. N. R. *ACS Nano* **2012**, *6*, 5635−5641.
(15) Late, D. J.; Huang, Y.; Liu, B.; Luo, J.; Acharya, J.; Shirodkar, S. N.; Luo, J.; Yan, A.; Charles, D.; Waghmare, U. V.; Dravid, V. P.; Rao, C. N. R. *ACS Nano* **2013**, *7*, 4879−4891.
(16) Kashid, R. V.; Late, D. J.; Chou, S. S.; Huang, Y.; De, M.; Joag, D. S.; More, M. A.; Dravid, V. P. *Small* **2013**, *9*, 2730−2734.
(17) (a) Rout, C. S.; Joshi, P. D.; Kashid, R. V.; Joag, D. S.; More, M. A.; Simbeck, A. J.; Washington, M.; Nayak, S. K.; Late, D. J. *Sci. Rep.* **2013**, *3*, 3282. (b) Braga, D.; Lezama, I. G.; Berger, H.; Morpurgo, A. F. *Nano Lett.* **2012**, *12*, 5218−5223. (c) Ratha, S.; Rout, C. S. *ACS Appl. Mater. Interfaces* **2013**, *5*, 11427.
(18) Georgiou, T.; Jalil, R.; Belle, B. D.; Britnell, L.; Gorbachev, R. V.; Morozov, S. V.; Kim, Y. J.; Gholinia, A.; Haigh, S. J.; Makarovsky, O.; Eaves, L.; Ponomarenko, L. A.; Geim, A. K.; Novoselov, K. S.; Mishchenko, A. *Nature Nanotechnol.* **2013**, *8*, 100−103.
(19) Berkdemir, A.; Gutiérrez, H. R.; Botello-Mendez, A.; Perea-Lopez, N.; Elas, A.N.; Chia, C.; Wang, B.; Crespi, V. H.; Lopez-Urıas, F.; Charlier, J.; Terrones, H.; Terrones, M. *Sci. Rep.* **2013**, *3*, 1755.
(20) Perea-López, N.; Elías, A. L.; Berkdemir, A.; Castro-Beltran, A.; Gutiérrez, H. R.; Feng, S.; Lv, R.; Hayashi, T.; López-Urías, F.; Ghosh, S.; Muchharla, B.; Talapatra, S.; Terrones, H.; Terrones, M. *Adv. Funct. Mater.* **2013**, *23*, 5511−5517.
(21) (a) Zhao, W.; Ghorannevis, Z.; Chu, L.; Toh, M.; Kloc, C.; Tan, P.; Eda, G. *ACS Nano* **2013**, *7*, 791−797. (b) Rout, C. S.; Joshi, P. D.; Kashid, R. V.; Joag, D. S.; More, M. A.; Simbeck, A. J.; Washington, M.; Nayak, S. K.; Late, D. J.; Nanocomposites. *Sci. Rep.* **2013**, *3*, 3282.
(22) Fang, H.; Chuang, S.; Chang, T. C.; Takei, K.; Takahashi, T.; Javey, A. *Nano Lett.* **2012**, *12*, 3788−3792.
(23) Liu, W.; Kang, J.; Sarkar, D.; Khatami, Y.; Jena, D.; Banerjee, K. *Nano Lett.* **2013**, *13*, 1983−1990.
(24) Tongay, S.; Zhou, J.; Ataca, C.; Lo, K.; Matthews, T. S.; Li, J.; Grossman, J. C.; Wu, J. *Nano Lett.* **2012**, *12*, 5576−5580.
(25) Ross, J. S.; Wu, S.; Yu, H.; Ghimire, N. J.; Jones, A. M.; Aivazian, G.; Yan, J.; Mandrus, D. G.; Xiao, D.; Yao, W.; Xu, X. *Nature Comm.* **2013**, *4*, 1474.
(26) Larentis, S.; Fallahazad, B.; Tutuc, E. *Appl. Phys. Lett.* **2013**, *101*, 223104.

(27) Kong, D.; Wang, H.; Cha, J. J.; Pasta, M.; Koski, K. J.; Yao, J.; Cui, Y. *Nano Lett.* **2013**, *13*, 1341−1347.
(28) Late, D. J.; Liu, B.; Luo, J.; Yan, A.; Matte, H. S. S. R.; Grayson, M.; Rao, C. N. R.; Dravid, V. P. *Adv. Mater.* **2012**, *24*, 3549−3554.
(29) Gutiérrez, H. R.; Perea-Lopez; Elías, A. L.; Berkdemir, A.; Wang, B.; Lv, R.; López-Urías, F.; Crespi, V. H.; Terrones, H.; Terrones, M. *Nano Lett.* **2013**, *13*, 3447.
(30) Zouboulis, E. S.; Grimsditch, M. *Phys. Rev. B* **1991**, *43*, 12490−12493.
(31) Lanzillo, N.A.; Birdwell, A.G.; Amani, M.; Crowne, F.J.; Shah, P. B.; Najmaei, S.; Liu, Z.; Ajayan, P. M.; Lou, J.; Dubey, M.; Nayak, S.K.; O'Regan, T.P. *Appl. Phys. Lett.* **2013**, *103*, 093102.
(32) Satyaprakash, S.; Gaur, A. P. S.; Ahmadi, M.; Guinel, M. J. F.; Katiyar, R. S. *J. Phys. Chem. C* **2013**, *117*, 9042−9047.
(33) Najmaei, S.; Ajayan, P. M.; Lou, J. *Nanoscale* **2013**, *5*, 9758−9763.